Research Article

Saima Noor*

Homogeneous–heterogeneous reactions in the colloidal investigation of Casson fluid

https://doi.org/10.1515/phys-2023-0174
received October 31, 2023; accepted December 18, 2023

Abstract: With particular attention to the effects of an electromagnetically induced resistive force on homogeneous–heterogeneous processes and the related homogeneous heat effects, the Casson fluid flow towards a stretching sheet at the magnetohydrodynamic stagnation point is investigated in detail. In this situation, the Laplace approach helps decipher the subtleties of the first-order kinetics governing the fluid's motion. Notably, the fluid dynamics are largely determined by the homogeneous behaviour expected in the surrounding environment, forming a strong correlation between catalyst temperature on the wall and surface activity. Using conventional differential systems, our analysis gains a great deal from the modified Laplace decomposition method, which allows non-linear systems to be computed and examined. In order to improve understanding, numerical findings are included, and graphs are skillfully used to examine the subtleties of different factors. The in-depth examination also includes the complicated patterns of concentration and temperature, providing insightful information on the intricate interactions between forces and effects in this dynamic system.

Keywords: Casson fluid, magnetohydrodynamics, modified Laplace decomposition method

Nomenclature

D_a	diffusion coefficient of A
D_b	diffusion coefficient of B
B_0	magnetic field
u_∞	free-flowing velocity
T	fluid temperature
Ω_p	heat capacity
λ	fluid relaxation time
α	thermal diffusivity
ΔH_h	uniform heat response
δ_A	coefficient of stoichiometry
ρ	fluid density
Ω_p	heat capacity
k_T	thermal conductivity
T_∞	ambient fluid temperature
Ω_∞	ambient fluid concentration
a, b	positive constant
u, v	velocity components in the x and y directions
A, B	reactants
k_1, k_2	reactions constants
Pr	Prandtl number
Sc	Schmidt number
γ	homogeneous parameter

1 Introduction

Flow experiments pertaining to non-linear materials are crucial in applied science and engineering. Many rheological models have been proposed to investigate the flow and heat transmission features. One of these materials is Casson fluid [1]. This model is widely used for various materials, including blood, chocolate, and honey. This model and some suspension flows have a close relationship. There is yield stress in this model. When tangential stress is less than the elastic limit, Casson fluid acts as if it were solid, and when stress exceeds yield stress, it begins to deform. Mehta *et al.* [2] investigated the Casson fluid behaviour under stress limit in a homogenous porous material enclosed by a tube was conducted. Hayat *et al.* [3] investigated the importance of Casson fluid flowing in a wavy channel with heat transmission and chemical reaction. The mixed convection effects were researched by Yasmin and Nisar [4] in Casson nano liquid with the chemical reaction. Another study [5] examines the non-Newtonian Casson fluid time-dependent magnetohydrodynamic (MHD) boundary layer flow along an infinite vertical plate under ramping temperature and concentration conditions.

* **Corresponding author: Saima Noor**, Department of Basic Sciences, Preparatory Year, King Faisal University, Al-Ahsa, 31982, Saudi Arabia, e-mail: snoor@kfu.edu.sa

The work tackles situations in which uniform wall temperature assumptions may not be sufficient in real-world settings such as electronic circuits, nuclear events, and materials processes.

Numerous chemically reactive systems, such as burning, biological structures, and catalysis, include homogeneous–heterogeneous reactions. Particularly puzzling is the relationship between homogeneous and heterogeneous processes. Without a catalyst, a reaction cannot occur; several reactions might not happen or develop slowly. Additionally, chemical reactions are employed in the production of ceramics, dispersion and fog formation, hydrometallurgical processes, food processing, and polymers.

This study covers a wide range of heat transfer and fluid dynamics scenarios. Jayavel *et al.* [6] use a viscoelastic hybrid nano fluid containing magnesium oxide (MgO) and silver (Ag) nanoparticles to study the combined effects of electric and Coriolis forces on heat transfer and rotating boundary layer flow. An empirical model is used to determine thermal conductivity. Akram *et al.* [7] emphasize using a modified Buongiorno model to peristaltically control electro-osmotic pumping of Ag–Au water-based hybrid nanofluids in a porous medium. In [8], gold nanoparticles are highlighted, and potential applications in the treatment of disease are explored through the introduction of a mathematical model for the two-dimensional motion of a pair stress nano fluid in an asymmetric microchannel. Latha *et al.* [9] explore the complex interplay in stagnation flow across the Hiemenz plane between MHD non-Newtonian fluid flow and thermal transfer. This research investigates the impact of a transverse static magnetic field on a ternary hybrid nanofluid coating through both theoretical and numerical analysis. When taken as a whole, these studies offer thorough insights into various fluidic and thermal conditions with possible uses in numerous sectors. Additionally, the MHD flow phenomena are important for both industry and physiology. As a result, the thermal performance enhancement of nanofluid with MHD was analyzed by Nawaz *et al.* [10]. Tain *et al.* [11] investigate radiation-induced two-dimensional unstable MHD boundary layer flow features. Hayat *et al.* [12] analyze the cumulative effects of heat radiation, convective conditions, and chemical reactions in flow caused by curved surfaces. Mahanthesh *et al.* [13] studied Soret and Dufour's effects in a three-dimensional MHD flow. An investigation of fluid flow with liquefaction and chemical change is conducted by Hayat *et al.* [14]. Flow caused by the elongated surface is used in many scientific processes, such as creating paper and fibres from polymer expulsion, drawing copper wires, and die forging and expulsion. A stretched sheet of metal that acts as a heat conductor was investigated by Cortell [15]. Aspects of heat transmission in magneto nanofluid flow across a stretchy, non-linear surface were addressed by Saleem *et al.* [16]. Hayat *et al.* [17] also analyzed heat generation/saturation, mixed convection, and double stratification in a thixotropic fluid flow state. Yasmeen *et al.* [18] described a magnetic dipole to control ferrofluid flow caused by a surface with a non-linear stretch. MHD nanomaterial flow and heat transmission across a stretchy radioactive surface were investigated by Sheikholeslami *et al.* [19]. Different aspects of MHD natural convection have been studied by many researchers. The Darcy–Forchheimer flow of a magneto-couple stress fluid across an inclined exponentially stretching sheet is theoretically simulated in [20]. For non-Newtonian features, it uses the Stokes pair stress model to investigate two thermal boundary conditions. The goal of the study is to provide a succinct understanding of the relationships between heat transfer, magneto-couple stress, and fluid flow for real-world uses. The flow and heat transmission properties of magneto-nanofluids over a curved stretched surface are studied numerically [21]. Because of their exceptional electrical and thermal conductivity, nanofluids have a lot of potential uses in industry and engineering. The study uses a convective boundary condition on the curved surface and accounts for the effects of viscous dissipation. The Keller-box approach [22] is used to get numerical solutions, which reveal two distinct solutions for opposing flows and one unique solution for aiding flows. Insights into the intricate interactions between stretching, permeability, and outside pressures on the fluid dynamics and thermal behaviour close to the stretched vertical permeable sheet are provided by the analysis, which focuses on comprehending the flow and heat transfer characteristics. Analysis of steady two-dimensional stagnation-point flow of an incompressible viscous fluid shows in relation to a flat deformable sheet stretched in its own plane at a velocity proportional to the distance from the stagnation point. Based on the link between the stretching velocity and the free stream velocity, the analysis reveals the production of both an inverted boundary layer and a boundary layer. The investigation also looks at the temperature distribution within the boundary layer and calculates the surface heat flux, which provides information about the fluid's thermal behaviour close to the deformable sheet [23]. Dong *et al.* [24] investigate the impact of magnetic fields on the sedimentation process of non-magnetic particles in ferrofluids. Sun *et al.* [25] focus on the rheological behaviour of shear-thickening fluids using carbon fibre and silica nanocomposites. Zheng *et al.* [26] delve into turbulent skin-friction drag reduction using annular dielectric barrier discharge plasma actuators. Additionally, Yin *et al.* [27] present a threat assessment methodology for aerial targets, employing an improved GRA-TOPSIS approach and three-way decisions in mathematical biosciences and engineering.

Scientists have developed many analytical and numerical techniques to address the inherent non-linearity present in a broad range of physical processes. The Laplace transform is frequently an efficient way to deal with linear systems, especially ones that are susceptible to periodic or discontinuous driving inputs. However, the complexity resulting from non-linearity makes the Laplace transform insufficient for dealing with non-linear equations. A number of strategies have been proposed recently to deal with these non-linear characteristics, including the Adomian decomposition method [28], which later led to the development of the Laplace decomposition algorithm, which was first presented by Khuri [29] and then further developed by Zheng [26]. This study aims to clarify the complex interaction between homogeneous and heterogeneous processes in the field of MHD by analyzing the dynamics of Casson fluid over a stretched surface. The Casson fluid because of its non-Newtonian properties provides a more accurate depiction of specific fluid behaviours. The use of Casson fluid allows for a detailed examination of the resulting phenomena. Our analysis specifically focuses on the impacts on velocity, distribution of temperature, composition of materials, drag forces, and rates of heat transfer. The governing partial differential equations that describe these occurrences are converted into a set of ordinary differential equations using suitable mathematical transformations. The objective of this research endeavour is to uncover fundamental knowledge about the complexities of MHD Casson fluid flow. This will lead to a more profound comprehension of the related physical phenomena and offer significant implications for practical uses.

2 Geometry of the flow problem

MHD steady flow is considered under the chemical reaction of Casson fluid. Compared to the magnetic field being applied, there is no consideration for the magnetic field induction. Furthermore, there is no electric field. The velocity of the sheet is extended in the direction of the x-axis ($u_w = ax$). The reaction in the isothermal cubic autocatalytic is assumed as follows [28]:

$$A + 2B \to 3B, \quad \text{rate} = k_1\Omega_a\Omega_b^2. \tag{1}$$

The overall system's temperature is constant. Isothermal reaction on a reactant surface is represented by

$$A \to B, \quad \text{rate} = k_2\Omega_a. \tag{2}$$

where (A) and (B) stand for the autocatalysis of chemical processes. (Ω_a) and (Ω_b) represent reaction concentrations, respectively, and the constants involved in the reaction are represented by (k_1) and (k_2). The reactant (B) is expected to be present, has a constant concentration, and is absent from the outer/external flow to satisfy physical necessities. Also assumed that reactant (A) concentration has a constant value (Ω_a). the relationship (1) shows that the reaction rate at the boundary layer's external edge is zero. Under the preceding presumption, thehe boundary layer equations, along with boundary conditions, are as follows (Figure 1):

$$\frac{\partial u}{\partial x} + \frac{\partial v}{\partial y} = 0, \tag{3}$$

$$u\frac{\partial u}{\partial x} + v\frac{\partial u}{\partial y} = u_e\frac{\mathrm{d}u_e}{\mathrm{d}x} + \nu\left(1 + \frac{1}{\beta}\right)\frac{\partial^2 u}{\partial y^2} + \frac{\sigma B_0^2}{\rho}(u_e - u), \tag{4}$$

$$u\frac{\partial T}{\partial x} + v\frac{\partial T}{\partial y} = \alpha\left(\frac{\partial^2 T}{\partial x^2} + \frac{\partial^2 T}{\partial y^2}\right) + \left(\frac{-\Delta H_h}{\delta_A}\right)\left(\frac{k_1\Omega_a\Omega_b^2}{\rho\Omega_p}\right), \tag{5}$$

$$u\frac{\partial \Omega_a}{\partial x} + v\frac{\partial \Omega_a}{\partial y} = D_A\left(\frac{\partial^2 \Omega_a}{\partial x^2} + \frac{\partial^2 \Omega_a}{\partial y^2}\right) - k_1\Omega_a\Omega_b^2, \tag{6}$$

$$u\frac{\partial \Omega_b}{\partial x} + v\frac{\partial \Omega_b}{\partial y} = D_B\left(\frac{\partial^2 \Omega_b}{\partial x^2} + \frac{\partial^2 \Omega_b}{\partial y^2}\right) + k_1\Omega_a\Omega_b^2, \tag{7}$$

$$\begin{aligned} &u = u_w = ax, v = 0, -kT\frac{\partial T}{\partial y} = k_2\Omega_a\left(\frac{-\Delta H_s}{\delta_A}\right), \\ &D_A\frac{\partial \Omega_a}{\partial y} = -D_B\frac{\partial \Omega_b}{\partial y} = k_2\Omega_a, y = 0, \end{aligned} \tag{8}$$

$$u = u_\infty \to ax, v \to 0, T \to T_\infty, \Omega_a \to \Omega_\infty, \Omega_b \to 0, y \to \infty. \tag{9}$$

Here, the velocity components are represented by u and v in the direction of x and y, respectively. Casson parameter is represented by (β), free-flowing velocity (u_∞), period for fluid relaxation (λ), magnetic field strength (B), temperature (T), thermal diffusivity (α), uniform heat response (ΔH_h), and coefficient of stoichiometry (δ_A) for species miscellaneous reactions are all factors that must be considered.

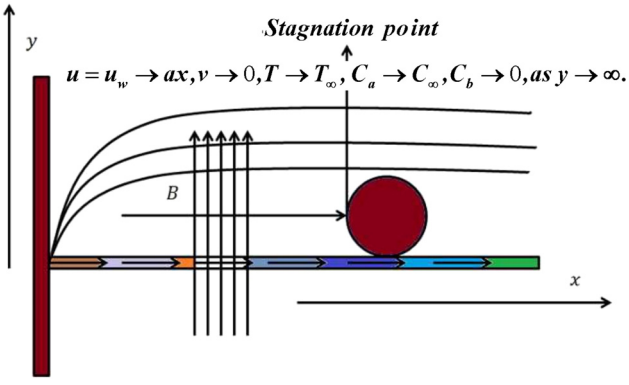

Figure 1: A schematic flow diagram.

Constant for dimensions are (a) and (b). (ρ) fluid density, (Ω_p) heat capacity, (k_T) thermal conductivity, (T_∞) ambient fluid temperature, and (Ω_∞) ambient fluid concentration. (D_a) and (D_b) diffusion coefficients of two species, (A) and (B). For brevity, we define

$$\eta = \sqrt{\frac{a}{v}}y, \phi = \sqrt{av}xf(\eta), \theta(\eta) = \frac{T - T_\infty}{\Delta T}, g(\eta) = \frac{\Omega_a}{\Omega_\infty}, h(\eta) = \frac{\Omega_b}{\Omega_\infty},$$

$$u = \frac{\partial \phi}{\partial y} = axf'(\eta), v = -\frac{\partial \phi}{\partial x} = -\sqrt{av}f(\eta), \quad \Delta T = T_w - T_\infty, \tag{10}$$

Eqs. (4)–(7) take the form when the incompressibility requirement is frequently satisfied

$$\left(1 + \frac{1}{\beta}\right)f''' + ff'' - f'^2 - M^2(f' - A) + A^2 = 0, \tag{11}$$

$$\frac{1}{\mathrm{Pr}}\theta'' + f\theta' + \gamma g h^2 = 0, \tag{12}$$

$$\frac{1}{\mathrm{Sc}}g'' + fg' - Kgh^2 = 0, \tag{13}$$

$$\frac{D}{\mathrm{Sc}}h'' + fh' + Kgh^2 = 0, \tag{14}$$

with boundary conditions,

$$f(0) = 0, f'(0) = 1, f'(\infty) = A, \tag{15}$$

$$\theta'(0) = -K_T g(0), \theta'(\infty) = 0, \tag{16}$$

$$g'(0) = -Dh'(0) = K_S g(0), g(\infty) = 1, h(\infty) = 0. \tag{17}$$

Here, Casson parameter is represented by (β), where $M\sqrt{\frac{\sigma\beta_0^2}{\rho a}}$ is a Prandtl number, a parameter of the magnetism. The parameter for homogeneous reaction heat is $\gamma = \left(k_1\left(\frac{\Delta H_h}{\delta_A}\right)\left(\frac{1}{\rho\Omega_p}\right)\left(\frac{\Omega_\infty^3}{a\Delta T}\right)\right)$ where Schmidt number is $\mathrm{Sc}\left(=\frac{v}{D_A}\right)$, $K\left(=\frac{k_1\Omega_\infty^2}{a}\right)$ stand for the homogeneous strength of reaction parameter, the ratio of diffusivity is $D\left(=\frac{D_B}{D_A}\right)$, $A = b/a$ represents ratio component, $K_T\left(=\frac{k_s\Omega_\infty}{k_T\Delta T}\left(\frac{\Delta H_S}{\delta_A}\right)\left(\frac{a}{v}\right)^{-\frac{1}{2}}\right)$ represents thermal conductivity in a homogenous reaction, and $K_S\left(=\frac{k_s}{D_A}\left(\frac{a}{v}\right)^{-\frac{1}{2}}\right)$ represents heterogeneous reaction component strength. We made the assumption that, (A) and (B) were comparable; (D_a) and (D_b) are then equal to unity.

$$g(\eta) + h(\eta) = 1. \tag{18}$$

3 Methodology

To explain the enhanced Laplace decomposition method's solution technique, we examine the traditional method of solving initial-value issues for non-linear, third-order, non-homogeneous ordinary differential equations, which is provided [30,31]

$$f''' + b_1(\eta)f'' + b_2(\eta)f' + b_3(\eta)f = g(\eta), \tag{19}$$

$$f(0) = \alpha, f(0) = \beta, f'(0) = \gamma. \tag{20}$$

We relate the Laplace transform on both sides of Eq. (19), while rendering to Laplace decomposition method [24,26]

$$s^3L[f] - s^2\alpha - s\beta - \gamma + L[b_1(\eta)f''] + L[b_2(\eta)f'] + L[b_3(\eta)f] = L[g(\eta)]. \tag{21}$$

Using the differentiation property of the Laplace transform, we obtain

$$L[f] = \frac{\alpha}{s} + \frac{\beta}{s^2} + \frac{\gamma}{s^3} + \frac{1}{s^3}L[g(\eta)] - \frac{1}{s^3}L[b_1(\eta)f'' + b_2(\eta)f' + b_3(\eta)f]. \tag{22}$$

The proposed approach acknowledges the result of the procedure

$$f = \sum_{n=0}^{\infty} f_n. \tag{23}$$

The non-linear terms can be expressed as follows:

$$g(\eta) = \sum_{n=0}^{\infty} A_n, \tag{24}$$

where (A_n) are Adomian polynomials of $f_0, f_1, f_2, f_3, \ldots, f_n$ which can be defined as

$$A_n = \frac{1}{n!}\frac{\mathrm{d}^m}{\mathrm{d}\lambda^n}\left[N\left(\sum_{i=0}^{\infty}\lambda^i f_i\right)\right]_{\overline{z}=0}, \quad n = 0, 1, 2, 3, \ldots \tag{25}$$

Applying Eqs. (23) and (24) in Eq. (22), we get

$$L\left[\sum_{n=0}^{\infty} f_n\right] = \frac{\alpha}{s} + \frac{\beta}{s^2} + \frac{\gamma}{s^3} + \frac{1}{s^3}L\left[\sum_{n=0}^{\infty} A_n\right] - \frac{1}{s^3}L\left[b_1(\eta)\sum_{n=0}^{\infty} f_n^N + b_2(\eta)\sum_{n=0}^{\infty} f_n + b_3(\eta)\sum_{n=0}^{\infty} f_n\right]. \tag{26}$$

After calculating on both sides of Eq. (26), and we get

$$L[f_0] = \frac{\alpha}{s} + \frac{\beta}{s^2} + \frac{\gamma}{s^3}, \tag{27}$$

$$L[f_1] = \frac{1}{s^3}L[A_0] - \frac{1}{s^3}L[b_1(\eta)f_0'' + b_2(\eta)f_0' + b_3(\eta)f_0], \tag{28}$$

$$L[f_2] = \frac{1}{s^3}L[A_1] - \frac{1}{s^3}L[b_1(\eta)f_1^N + b_2(\eta)f_1' + b_3(\eta)f_1] \tag{29}$$

In the recursive relation

$$L[f_{m+1}] = \frac{1}{s^3}L[A_m] - \frac{1}{s^3}L[b_1(x)f_m'' + b_2(x)f_m' + b_3(x)f_m], m \geq 0. \tag{30}$$

When we use the inverse Laplace transform, we obtain

$$f_0(x) = H(x), \tag{31}$$

$$f_{n+1}(\eta) = L^{-1}\left[\frac{1}{s^3}L[A_n] - \frac{1}{s^3}L[b_1(\eta)f_n'' + b_2(x)f_n' + b_3(\eta)f_n]\right], \quad n = 0,1,2,3,... \tag{32}$$

One term that arises from source terms and incorporates the initial circumstances is represented by the variable $H(\eta)$. The modified Laplace decomposition method (MLDM) [28] suggests that $H(\eta)$ defined above in (31) can be decomposed as $H_0(\eta)$ and $H_1(\eta)$ like as

$$H(\eta) = H_0(\eta) + H_1(\eta). \tag{33}$$

The first explanation is authoritative because noisy oscillation is consistently produced throughout repeated iterations when the prime is present in Eq. (30) as the initial response. We suggest the following change as an alternative to the iterative procedure provided by Eqs. (30) and (31):

$$f_0(\eta) = H_0(\eta), \tag{34}$$

$$f_1(\eta) = H_1(\eta) + L^{-1}\left[\frac{1}{\eta}L[A_0] - \frac{1}{s^3}L[b_1(\eta)f_0'' + b_2(\eta)f_0' + b_3(\eta)f_0]\right], \tag{35}$$

$$f_{n+1}(\eta) = L^{-1}\left[\frac{1}{s}L[A_n] - \frac{1}{s}L[b_1(\eta)f_n^* + b_2(\eta)f_n' + b_3(\eta)f_0]\right], \quad n \geq 1. \tag{36}$$

After applying the aforementioned expansions, the modified Adomian polynomials (A_n) are organized to take the following form from the simple analytic non-linearity, leading to the conclusion that the MLDM was significantly dependent on $H_0(\eta)$ and $H_1(\eta)$ optimal values:

$$A_0 = \frac{1}{0!}\frac{d^0}{d\lambda^0}\left[N\left(\sum_{i=0}^{0}\lambda^i f_i\right)\right] = N(f_0), \tag{37}$$

$$A_1 = \frac{1}{1!}\frac{d^1}{d\lambda^1}\left[N\left(\sum_{i=0}^{1}\lambda^i f_i\right)\right] = \frac{1}{1!}\frac{d^1}{d\lambda^1}[N(\lambda^0 f_0 + \lambda^1 f_1)] = [N'(\lambda^0 f_0 + \lambda^1 f_1)](f_1) = f_1 N'(f_0), \tag{38}$$

$$\begin{aligned} A_2 &= \frac{1}{2!}\frac{d^2}{d\lambda^2}\left[N\left(\sum_{i=0}^{2}\lambda^i f_i\right)\right] \\ &= \frac{1}{2!}\frac{d^2}{d\lambda^2}[N(\lambda^0 f_0 + \lambda^1 f_1 + \lambda^2 f_2)], \\ &= \frac{1}{2!}\frac{d}{d\lambda}[N'(\lambda^0 f_0 + \lambda^1 f_1 + \lambda^2 f_2)(f_1 + 2\lambda f_2)], \\ &= \frac{1}{2!}[N'(\lambda^0 f_0 + \lambda^1 f_1 + \lambda^2 f_2)(2f_2)], \end{aligned} \tag{39}$$

$$A_3 = f_3 N'(f_0) + f_1 f_2 N''(u_0) + \frac{1}{3!}f_1^3 N'''(u_0), \tag{40}$$

where $N = f_{n+1}(\eta)$, and similarly, we have found other polynomials

4 Results and discussions

Many important parameters influence the flow, temperature, and chemical composition of the fluid. In Figures 2–8, the temperature transfer rate and heat transfer rate are shown to be dependent on the ratio of the Casson fluid parameter and the Prandtl number, as well as the magnetic parameter and Prandtl number for homogeneous reactions.

Looking more closely at Figure 2, we can observe that the velocity profile shows a concave-down form for ($A > 1$), indicating that stagnation velocity exceeds stretching velocity. On the other hand, the velocity profile concave-ups when ($A < 1$), indicating that stretching velocity outweighs stagnation velocity. These discoveries provide important new information about the fluid dynamics related to various values of parameter (A). The physical interpretation of the results is further enhanced by the concavity of the velocity profile, which offers a concrete knowledge of the interaction between stretching and stagnation velocities.

Figure 3 depicts the effect of a magnetic parameter on a velocity field. It turns out that a higher (M) estimation

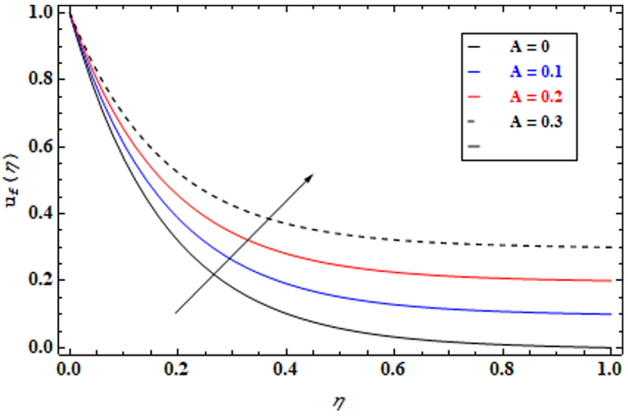

Figure 2: Variation of (A) on (u_f) for different values of $\beta = M = 0.2$, Pr = 0.8, $\gamma = 0.7$, Sc = 0.4.

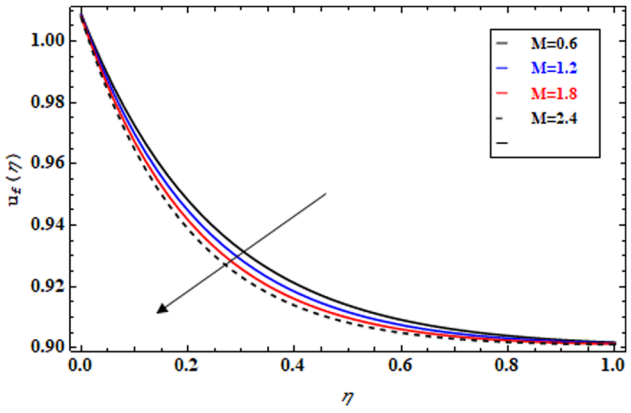

Figure 3: Variation of (M) on (u_f) for different values of $\beta = A = 0.2,\ \mathrm{Pr} = 0.8,\ \gamma = 0.7,\ \mathrm{Sc} = 0.4$.

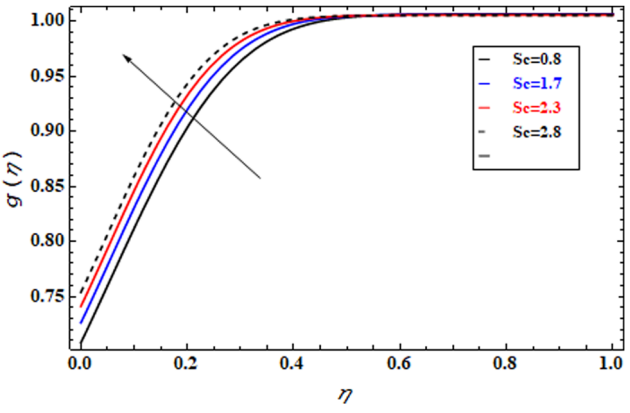

Figure 6: Variation of (Sc) on (g) for different values of $\beta = M = 0.2,\ \mathrm{Pr} = 0.8,\ A = 0.2,\ \gamma = 0.7$.

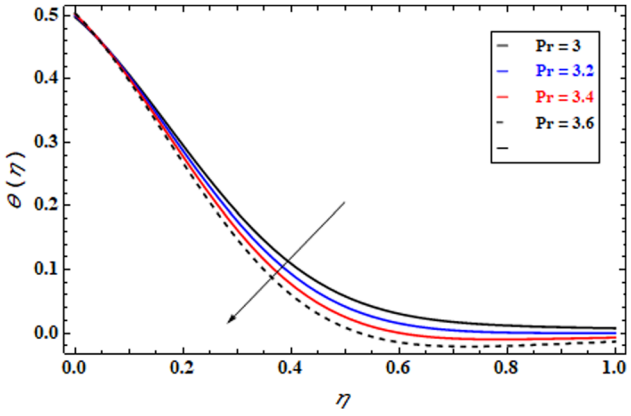

Figure 4: Variation of (Pr) on (θ) for different values of $\beta = M = 0.2,\ \mathrm{Pr} = 0.8,\ \gamma = 0.7,\ \mathrm{Sc} = 0.4$.

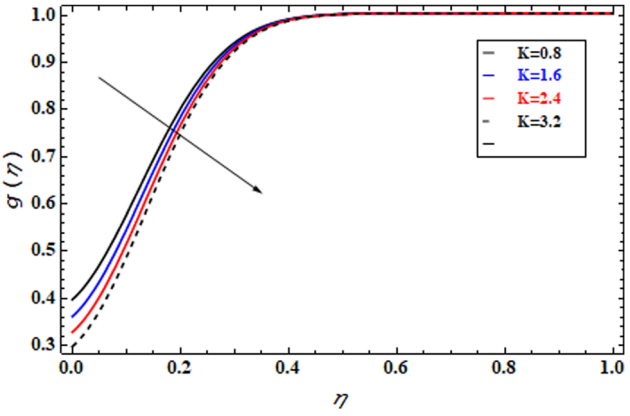

Figure 7: Variation of (K) on (g) for different values of .

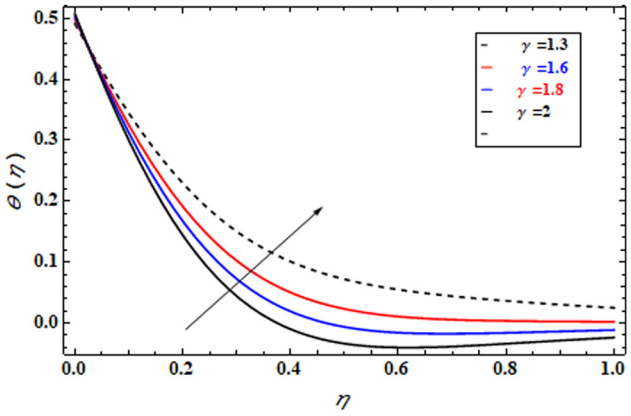

Figure 5: Variation of (γ) on (θ) for different values of $\beta = M = 0.2,\ \mathrm{Pr} = 0.8,\ A = 0.2,\ \mathrm{Sc} = 0.4$.

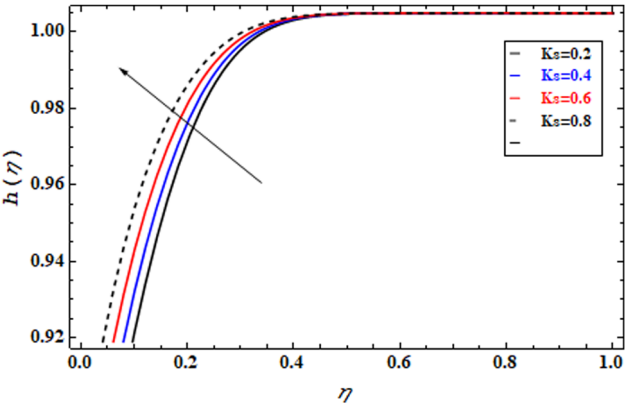

Figure 8: Variation of (K_s) on (h) for different values of $\beta = M = 0.2,\ \mathrm{Pr} = 0.8,\ A = 0.2,\ \mathrm{Sc} = 0.4$.

Table 1: Numerical values of drag force $-(1 + 1/\beta)f''(0)$ and heat transfer rate $-\theta'(0)$ for different values of β, γ, Pr, Sc, M, and (A)

(β)	(γ)	(Pr)	(Sc)	(M)	(A)	$-(1 + 1/\beta)f''(0)$	$-\theta'(0)$
0.5	0.2	0.8	0.6	0.4	0.7	1.48778	0.398315
0.8						1.28164	0.400273
1.5						1.09619	0.401999
2.0						1.03747	0.403041
1.0	0.0					1.30452	0.383969
	0.2					1.20549	0.400992
	0.4					1.00575	0.423584
	0.6					0.72445	0.445054
		0.3				1.14878	0.329744
		0.7				1.19948	0.392272
		1.2				1.22077	0.425225
		2.0				1.23461	0.450830
			0.0			1.23236	0.452028
			0.3			1.21874	0.426086
			0.7			1.20115	0.392809
			1.0			1.18836	0.368778
				0.0		1.29840	0.394821
				0.5		1.18313	0.402408
				1.0		1.07574	0.408860
				1.5		0.974474	0.414442
					0.2	1.24049	0.152594
					0.5	1.21712	0.318102
					1.0	1.19186	0.498457
					1.5	1.17567	0.614761

slows down the flow, resulting in a lower momentum layer in the flow domain. This behaviour suggests that the interaction of a magnetic field with fluid results in the formation of a Lorentz force, a constraining force that slows the fluid's speed. Figure 4 depicts how the Prandtl number Pr affects the temperature field. As the Prandtl number (Pr) increases, the thermal boundary layer decreases. As a result, the heat transfer rate decreases, lowering the fluid temperature, to investigate how the temperature field is affected by the homogeneous reaction heat parameter. Figure 5 depicts a conceptual sketch of the dynamic interaction between the homogeneous reaction heat parameter and the temperature field. The graph shows that as the homogeneous reaction heat parameter increases, the temperature field grows proportionally. From a physical perspective, this implies that the system's thermal behaviour is directly influenced by the strength or rate of the homogeneous response. An increased temperature field is associated with a greater homogenous reaction heat parameter, suggesting that the reaction heat has a significant effect on the overall thermal profile. Figure 6 depicts the effect of (Sc) on the concentration profile. By raising the values of (Sc), the concentration profile is improved. It is because the rate of momentum diffusivity rises, which guarantees an improvement in concentration. Concentration distributions are affected by (K) and (K_s) are shown in Figures 7 and 8. It should be noted that the two parameters of the concentration field behave differently. It is obvious that as the heterogeneous reaction parameter grows, the boundary layer thickness decreases. Table 1 presents a thorough examination of the effects of physical characteristics of drag force and heat transfer rate for a subset of values. Table 2 indicates that series solutions suggest convergence at the 20th order of approximations. A comparison of the current results with previous numerical solutions is shown in Table 3. The results show remarkable consistency, suggesting a high degree of agreement across the options presented.

Table 2: Convergence of MLADM for different orders of approximations, when $\beta = 1.0$, $\gamma = 0.2$, Pr = 0.8, Sc = 0.6, $M = 0.4$, $A = 0.5$

Order	$-f''(0)$	$-\theta'(0)$
1	0.618824	0.389381
5	0.602249	0.401168
10	0.602764	0.400977
15	0.602742	0.400994
20	0.602744	0.400992
25	0.602744	0.400992
30	0.602744	0.400992

Table 3: Comparison for values of $f''(0)$ with Ishak *et al.* [22] and Mahapatra and Gupta [23] for different values of (A) when $\beta \to \infty$

(A)	Ref. [22]	Ref. [23]	MLADM results
0.01	−0.9980		−0.998024
0.10	−0.9694	−0.9694	−0.969386
0.20	−0.9181	−0.9181	−0.918107
0.50	−0.6673	−0.9181	−0.667263
2.00	2.0175	2.0175	2.01756
3.00	4.7294	4.7294	4.72963

5 Conclusions

To summarize, this study not only clarifies the existing model's understanding of temperature dynamics, but it also presents opportunities for future research and practical applications. It is essential to continuously explore these possibilities in order to increase our understanding of homogeneous and heterogeneous reactions within the colloidal framework of Casson fluid and its broader ramifications.

The following is a main summary of the current analysis:

- As the magnetic parameter increases, the velocity field increases.

- For higher values of (Pr), the temperature profile decreases.
- First-order kinetics governs the homogenous reactions in the domain fluid and the isothermal cubic autocatalytic kinetics.
- It is established that chemical reactions include a combination of heat and mass exchange.

In the future, there is a significant opportunity for additional investigation and improvement of this model. Subsequent inquiries may explore the intricate impacts of supplementary variables, such as (A, M, Pr, γ, Sc, K, K_s), in order to attain a more thorough comprehension of the fundamental mechanisms. This work has significant consequences that go beyond theoretical comprehension, opening up opportunities for practical implementation in specific disciplines or industries. For example, analysis of colloidal stability in industries such as pharmaceuticals and cosmetics, development and enhancement of controlled release systems through design and optimization, nanoparticle functionalization for specific purposes, manipulation of rheological characteristics for sectors such as coatings and lubricants, biomedical research focused on studying interactions within fluid environments that do not follow Newton laws of motion, applications in the field of environmental science, such as ways for cleaning up pollutants in fluid settings that do not follow Newton's laws of motion.

Acknowledgments: The author acknowledges the support of the Deanship of Scientific Research, Vice Presidency for Graduate Studies and Scientific Research, King Faisal University, Saudi Arabia [Grant No. 5382].

Funding information: This work was supported by the Deanship of Scientific Research, Vice Presidency for Graduate Studies and Scientific Research, King Faisal University, Saudi Arabia [Grant No. 5382].

Author contributions: The author has accepted responsibility for the entire content of this manuscript and approved its submission.

Conflict of interest: The author states no conflict of interest.

References

[1] Casson N. A flow equation for pigment oil suspensions of the printing ink type. Rheology of Disperse Systems, Pergamonpress. New York; 1959. p. 84–104.

[2] Dash RK, Mehta KN, Jayaraman G. Effect of yield stress on the flow of a Casson fluid in a homogeneous porous medium bounded by a circular tube. Appl Sci Res. 1996;57:133–49.

[3] Hayat T, Yasmin H, Alyami M. Soret and Dufour effects in peristaltic transport of physiological fluids with chemical reaction: A mathematical analysis. Comp Fluids. 2014;89:242–53.

[4] Yasmin H, Nisar Z. Mathematical analysis of mixed convective peristaltic flow for chemically reactive Casson nanofluid. Mathematics. 2023;11:2673.

[5] Das S, Banu AS, Jana RN. Delineating impacts of non-uniform wall temperature and concentration on time-dependent radiation-convection of Casson fluid under magnetic field and chemical reaction. World J Eng. 2021;18(5):780–95.

[6] Jayavel P, Tripathi D, Anwar Beg O, Tiwari AK, Kumar R. Thermo-electrokinetic rotating non-Newtonian hybrid nanofluid flow from an accelerating vertical surface. Heat Transf. 2022 Mar;51(2):1746–77.

[7] Akram J, Akbar NS, Tripathi D. A theoretical investigation on the heat transfer ability of water-based hybrid (Ag–Au) nanofluids and Ag nanofluids flow driven by electroosmotic pumping through a microchannel. Arab J Sci Eng. 2021 Mar;46:2911–27.

[8] Sridhar V, Ramesh K, Tripathi D, Vivekanand V. Analysis of thermal radiation, Joule heating, and viscous dissipation effects on blood-gold couple stress nanofluid flow driven by electroosmosis. Heat Transf. 2022 Jul;51(5):4080–101.

[9] Latha KB, Reddy MG, Tripathi D, Bég OA, Kuharat S, Ahmad H, et al. Computation of stagnation coating flow of electro-conductive ternary Williamson hybrid GO-AU-Co_3O_4/EO nanofluid with a Cattaneo–Christov heat flux model and magnetic induction. Sci Rep. 2023 Jul;13(1):10972.

[10] Nawaz M, Nazir U, Saleem S, Alharbi SO. An enhancement of thermal performance of ethylene glycol by nano and hybrid nanoparticles. Phys A: Stat Mech Appl. 2020;551:124527.

[11] Tian XY, Li BW, Zhang JK. The effects of radiation optical properties on the unsteady 2D boundary layer MHD flow and heat transfer over a stretching plate. Int J Heat Mass Transf. 2017;105:109–23.

[12] Hayat T, Rashid M, Imtiaz M, Alsaedi A. MHD convective flow due to a curved surface with thermal radiation and chemical reaction. J Mol Liq. 2017;225:482–9.

[13] Mahanthesh B, Gireesha BJ, Gorla RSR. Non-linear radiative heat transfer in MHD three-dimensional flow of water based nanofluid over a non-linearly stretching sheet with convective boundary condition. J Nigerian Math Socie. 2016;35(1):178–98.

[14] Hayat T, Khan MI, Alsaedi A, Khan MI. Homogeneous-heterogeneous reactions and melting heat transfer effects in the MHD flow by a stretching surface with variable thickness. J Mol Liq. 2016;223:960–8.

[15] Cortell R. Flow and heat transfer in a moving fluid over a moving flat surface. Theor Comput Fluid Dynam. 2007;21:435–46.

[16] Saleem S, Al-Qarni MM, Nadeem S, Sandeep N. Convective heat and mass transfer in magneto Jeffrey fluid flow on a rotating cone with heat source and chemical reaction. Commun Theor Phys. 2018;70:534. doi: 10.1088/0253-6102/70/5/534.

[17] Hayat T, Waqas M, Khan MI, Alsaedi A. Analysis of thixotropic nanomaterial in a doubly stratified medium considering magnetic field effects. Int J Heat Mass Transf. 2016;102:1123–9.

[18] Yasmeen T, Hayat T, Khan MI, Imtiaz M, Alsaedi A. Ferrofluid flow by a stretched surface in the presence of magnetic dipole and homogeneous-heterogeneous reactions. J Mol Liq. 2016;223:1000–5.

[19] Sheikholeslami M, Ganji DD, Javed MY, Ellahi R. Effect of thermal radiation on magnetohydrodynamics nanofluid flow and heat

transfer by means of two phase model. J Magn Magn Mater. 2015;374:36–43.
[20] Das S, Ali A, Jana RN. Darcy–Forchheimer flow of a magneto-radiated couple stress fluid over an inclined exponentially stretching surface with Ohmic dissipation. World J Eng. 2021;18(2):345–60.
[21] Das S, Ali A, Jana RN. Numerically framing the impact of magnetic field on nanofluid flow over a curved stretching surface with convective heating. World J Eng. 2021;18(6):938–47.
[22] Ishak A, Nazar R, Arifin NM, Pop I. Mixed convection of the stagnation-point flow towards a stretching vertical permeable sheet. Malays J Math Sci. 2007;1(2):217–26.
[23] Mahapatra TR, Gupta AS. Heat transfer in stagnation-point flow towards a stretching sheet. Heat Mass Transf. 2002 Jun;38(6):517–21.
[24] Dong Z, Li X, Yamaguchi H, Yu P. Magnetic field effect on the sedimentation process of two non-magnetic particles inside a ferrofluid. J Magn Magn Mater. 2024;589:171501. doi: 10.1016/j.jmmm.2023.171501.
[25] Sun L, Liang T, Zhang C, Chen J. The rheological performance of shear-thickening fluids based on carbon fiber and silica nanocomposite. Phys Fluids. 2023;35(3):32002. doi: 10.1063/5.0138294.
[26] Zheng B, Lin D, Qi S, Hu Y, Jin Y, Chen Q, et al. Turbulent skin-friction drag reduction by annular dielectric barrier discharge plasma actuator. Phys Fluids. 2023;35(12):125129. doi: 10.1063/5.0172381.
[27] Yin Y, Zhang R, Su Q. Threat assessment of aerial targets based on improved GRA-TOPSIS method and three-way decisions. Math Biosci Eng. 2023;20(7):13250–66. doi: 10.3934/mbe.2023591.
[28] Adomian G. Solving frontier problems of physics: The decomposition method. Boston: Kluwer Academic Publication; 1994.
[29] Khuri SA. A Laplace decomposition algorithm applied to a class of nonlinear differential equations. J Appl Math. 2001;1(4):141–55.
[30] Yusufoglu E. Numerical solution of Duffing equation by the Laplace decomposition algorithm. Appl Math Comput. 2006;177:572–80.
[31] Merkin JH. Amodel for isothermal homogeneous-heterogeneous reactions in boundarylayer flow. Math Comput Model. 1996;24:125–36.